Biosensors and Bioelectronics 50 (2013) 217–223

Contents lists available at SciVerse ScienceDirect

Biosensors and Bioelectronics

journal homepage: www.elsevier.com/locate/bios

rhEPO/EPO discrimination with ultrasensitive electrochemical biosensor based on sandwich-type nano-Au/ZnO sol–gel/nano-Au signal amplification

Liqun Zhang [a,1], Yunxia Wang [a,1], Jingjing Wang [b], Jianfeng Shi [c], Kun Deng [a], Weiling Fu [a,*]

[a] Department of Laboratory Medicine, Southwest Hospital, Third Military Medical University, Chongqing 400038, PR China
[b] Department of Laboratory Medicine, Xinqiao Hospital, Third Military Medical University, Chongqing 400037, PR China
[c] The 26th Research Institute, Chinese Electronic Scientific and Technical Group Company, Chongqing 400060, PR China

ARTICLE INFO

Article history:
Received 25 March 2013
Received in revised form
10 June 2013
Accepted 19 June 2013
Available online 27 June 2013

Keywords:
Electrochemical
Sensor
Erythropoietin (EPO)
Signal amplification
Nano-Au

ABSTRACT

This research established a non-labeled electrochemical biosensor for discrimination of recombinant human erythropoietin (rhEPO) and endogenous erythropoietin (EPO). We prepared a glassy carbon electrode (GCE) modified by a unique sandwich-like nano-Au/ZnO sol–gel/nano-Au compound membrane for signal amplification. The porous sol–gel structure facilitates protein activity maintenance and thermostability. Nano-Au is characterized by a large specific surface area, high surface activity, high absorbability, and good electro-conductivity and biocompatibility. By combining the advantages of both ZnO sol–gel and nano-Au, the amount of erythropoietin receptor (EPOR) increased substantially, and electron transfer of EPOR protein and electrode surface increased accordingly. In the present study, the effects of experimental conditions such as nano-Au electrodeposition time and nano-Au concentration were investigated by cyclic voltammetry, and the process of GCE modification was characterized electrochemically. We successfully developed a new method for electrochemical detection of trace rhEPO/EPO. More importantly, the response current change (ΔI) of the nano-Au/ZnO sol–gel/nano-Au modified GCE increases 3-fold when compared with that of the unmodified electrode and the sensor detection sensitivity increases significantly. In conclusion, this electrochemical biosensor is simple to prepare and allows fast, accurate, and specific detection of trace rhEPO in clinical monitoring and stimulant discrimination.

1. Introduction

Biosensors utilize molecules recognizing organism elements as sensitive elements as well as physical transducers (Takulapalli, 2010). Electrochemical biosensors are one of the focuses of research in biological diagnosis due to their high sensitivity and selectivity (Tothill, 2009; Wei et al., 2009). An electrochemical biosensor is typically composed of biological molecule recognition elements and a signal transformer (Cash et al., 2009; Lubin and Plaxco, 2010). Biological molecule recognition elements are biological sensitive membranes fabricated by fixing organism elements or organisms as sensitive elements onto a matrix, and the signal transformer is typically an electrode (Cash et al., 2009; Zhang et al., 2010). The potential difference between the electrode surface and electrolyte solution changes when electrochemical reactions of chemical elements in the base electrolyte solution change. Sensor's signal transformer transforms such change into analyte concentration related signal output, which is then processed and displayed by an electric signal acquisition and analysis system. The major factors that limit the performance of sensor detection include narrow linear detection range and low detection sensitivity.

Signal amplification is crucial to detect target molecules at very low concentrations. Signal amplification is widely used in trace detection of pathogenic microorganisms, early diagnosis of disease, gene mutation detection, and accurate discriminations of sports stimulants (Liu et al., 2011; Jeong et al., 2012). Electrode modification and biological molecule fixation methods are useful for signal amplification of electrochemical biosensors. Electrochemical sensors using sol–gel as a matrix are novel biosensors, which utilize electrostatic interactions to fix protein onto the surface of a glassy carbon electrode (GCE), and allow real-time electrochemical detection of protein binding reactions. The sol–gel facilitates maintenance of protein bioactivity, and it is also highly porous, thermally stable, chemically inert and biocompatible. Some

* Corresponding author. Tel.: +86 23 687 544 29; fax: +86 23 654 609 09.
E-mail addresses: zlqtmmu@gmail.com (L. Zhang), weilingfu@yahoo.com (W. Fu).
[1] These authors contributed equally to the study.

0956-5663/$ - see front matter © 2013 Elsevier B.V. All rights reserved.
http://dx.doi.org/10.1016/j.bios.2013.06.038

non-silicone sol–gel materials have been used to modify electrochemical sensor surfaces, and ZnO is a readily available non-silicone sol–gel material. Due to its high isoelectric point, ZnO can absorb proteins having a low isoelectric point (Gu et al., 2011). The ZnO sol–gels exhibits good biocompatibility, and its surface porosity makes it an ideal protein fixation matrix (Wei et al., 2010; Lei et al., 2011; Arya et al., 2012; Palanisamy et al., 2012; Zhao et al., 2013).

Based on long-term research on biosensors (Wang et al., 2009; Deng et al., 2013), we prepared an electrochemical biosensor which allows fast and accurate discrimination of rhEPO/EPO by utilizing the minor difference in isoelectric point between rhEPO and EPO (Lasne et al., 2002, 2007; Mallorqui et al., 2008). We observed that at low rhEPO/EPO concentrations, the peak current changes were small in cyclic voltammograms (CV). In order to further increase sensor's detection sensitivity for fast and accurate detection of trace rhEPO/EPO, we introduced a nano-Au/ZnO sol–gel/nano-Au sandwich-like compound membrane in this detection system, with the intention to further amplify the detection signal of very low concentrations of analytes.

Signal amplification is critical to increase biosensor's detection sensitivity, and it is realized primarily through utilizing multifunctional nanoparticles, enzyme labeling and sandwich-like analysis (Li et al., 2010; Tan et al., 2010; Liu et al., 2013). Due to their unique physical and chemical properties, nanoparticles have a broad applicability in the biosensor field (Li F. et al., 2011). Nano-Au is characterized by a large specific surface area, very high surface activity, strong biological molecule absorbability, and good electro-conductivity and biocompatibility (Yeom et al., 2011; Lee et al., 2012); thus, it allows more EPOR absorption on the surface of the modified electrode, while maintaining EPOR bioactivity. In the present study, a nano-Au/ZnO sol–gel/nano-Au-modified electrode was prepared by combining the benefits of ZnO sol–gel and nano-Au. In brief, a layer of nano-Au was electrodeposited onto the electrode surface, and then a second layer of nano-Au was electrodeposited onto the electrode surface through ZnO sol–gel electrostatic absorption of nano-Au, thus forming a nano-Au/ZnO sol–gel/nano-Au-modified sensor electrode surface. The results demonstrate that EPOR fixation using the nano-Au/ZnO sol–gel/nano-Au sandwich method greatly increased electron transfer on the electrode surface, thus increasing sensor's ΔI and sensitivity and allowing accurate detection of trace rhEPO/EPO.

2. Experimental

2.1. Reagents and materials

Lithium hydroxide ($LiOH \cdot H_2O$), zinc acetate ($Zn(OAc)_2 \cdot 2H_2O$), absolute alcohol, nitric acid, acetone, potassium ferricyanide, PBS powder, and potassium ferrocyanide were commercially available analytically as pure products and were purchased from Shanghai Sangon Bioengineering Co., Ltd. (Shanghai, China); $K_3[Fe(CN)_6]$ and $K_4[Fe(CN)_6]$ were purchased from Chongqing Dongfang Reagents Factory (Chongqing, China); $HAuCl_4$ was purchased from Beijing Bailingwei Chemical Technology Co., Ltd. (Beijing, China). The GCE, the saturated calomel electrode, the platinum electrode and 0.3 μm, 0.05 μm Al_2O_3 powder were purchased from AidaHengsheng Tech. Co., Ltd. (Tianjin, China). EPO and EPOR were purchased from Novus Biologicals (USA), and rhEPO standard preparation from Abnova (USA). Bovine serum albumin (BSA) was purchased from Sigma Chemical Co. (St. Louis, MO, USA). IgA, IgG and IgM antibodies were purchased from Beyotime Institute of Biotechnology (Nantong, Jiangsu, China).

2.2. Instrumentation

CHI760D electrochemical workstation was purchased from Shanghai Chenhua Instruments Co., Ltd. (Shanghai, China). The scanning electron micrograph was taken with field emission scanning electron microscopy (FESEM) LEO SUPRA 35 (Oberkochen, Germany). KQ-5200B ultrasound washer (Kunshan Ultrasound Instruments Co., Ltd., Jiangsu, China), ZD-2 automatic electric potential titrimeter (Shanghai Jingke Leici Co., Ltd., China) were used. An electrochemical biosensor detection system was fabricated using the home-made EPOR-modified GCE as working electrode, a saturated calomel electrode as reference electrode, and a platinum electrode as counter electrode.

2.3. Preparation of ZnO sol–gel

1.10 g (5 mmol) of Zn $(CH_3COO)_2 \cdot 2H_2O$ was added to 50 mL of absolute alcohol. The mixture was stirred vigorously at 80 °C for 20 min to dissolve Zn $(CH_3COO)_2 \cdot 2H_2O$. Then, 0.29 g (7 mmol) $LiOH \cdot H_2O$ was added to 50 mL of absolute alcohol, followed by sonication at room temperature to facilitate dissolution. Afterwards, the $Zn(CH_3COO)_2 \cdot 2H_2O$ alcohol solution and the $LiOH \cdot H_2O$ alcohol solution were mixed and stirred vigorously for 40 min. 1.0 mol L^{-1} NaOH was added to the final solution to adjust the pH to 9.

2.4. Preparation of the modified electrode

GCE (3 mm in diameter) was burnished first with 0.3 μm, and then with 0.05 μm Al_2O_3 powder. Between burnishes, the electrodes were washed first with purified water, and then in an ultrasound bath with nitric acid, acetone and ultrapure water each for 5 min. After each wash, the electrodes were air-dried.

After each wash, the electrode was immersed in 10 mmol L^{-1} $HAuCl_4$ for a 60 s electrodeposition at constant potential. After washing in ultrapure water, ZnO sol–gel solution containing 20 μl EPOR (EPOR solution volume/ZnO sol–gel solution volume, 1/1) was dripped onto the nano-Au modified electrode surface and then placed at 4 °C for 10 h. After washing in ultrapure water, the modified electrode was immersed in 10 mmol L^{-1} $HAuCl_4$ solution for a 30 s electrodeposition at constant potential. After washing in ultrapure water, the modified electrode was immersed in 0.25% BSA solution for 1 h at 4 °C to block nonspecific absorptive sites. Scheme 1 may illustrate electrode modification. Prior to use, the modified electrode was suspended in PBS solution at 4 °C away from light.

2.5. Hybridization reaction and electrochemical measurements

Nano-Au/ZnO sol–gel EPOR/nano-Au modified electrodes were immersed in different concentrations rhEPO or EPO solution, and incubated for 20 min at room temperature. The electrochemical sensor detection system was connected to the electrochemical workstation via a dedicated cable. The electric potential scanned ranged from −0.3 V to 0.7 V in 0.05 mol L^{-1} phosphate buffer solution (PBS, pH 7.4, containing 2 mmol L^{-1} $K_3Fe(CN)_6/K_4Fe(CN)_6$ as supporting electrolytes), and the electric potential scanning speed was 50 mV s^{-1}.

For electrochemical biosensor detection, the initial peak current measured by the EPOR-modified electrode was recorded as I_0; the peak current measured following the EPOR–rhEPO/EPO hybridization reaction was recorded as I; thus, the peak current change was expressed as $\Delta I = I - I_0$. In this study, it was presumed that a higher ΔI value represents a larger quantity of rhEPO/EPO bound to EPOR on the electrode surface.

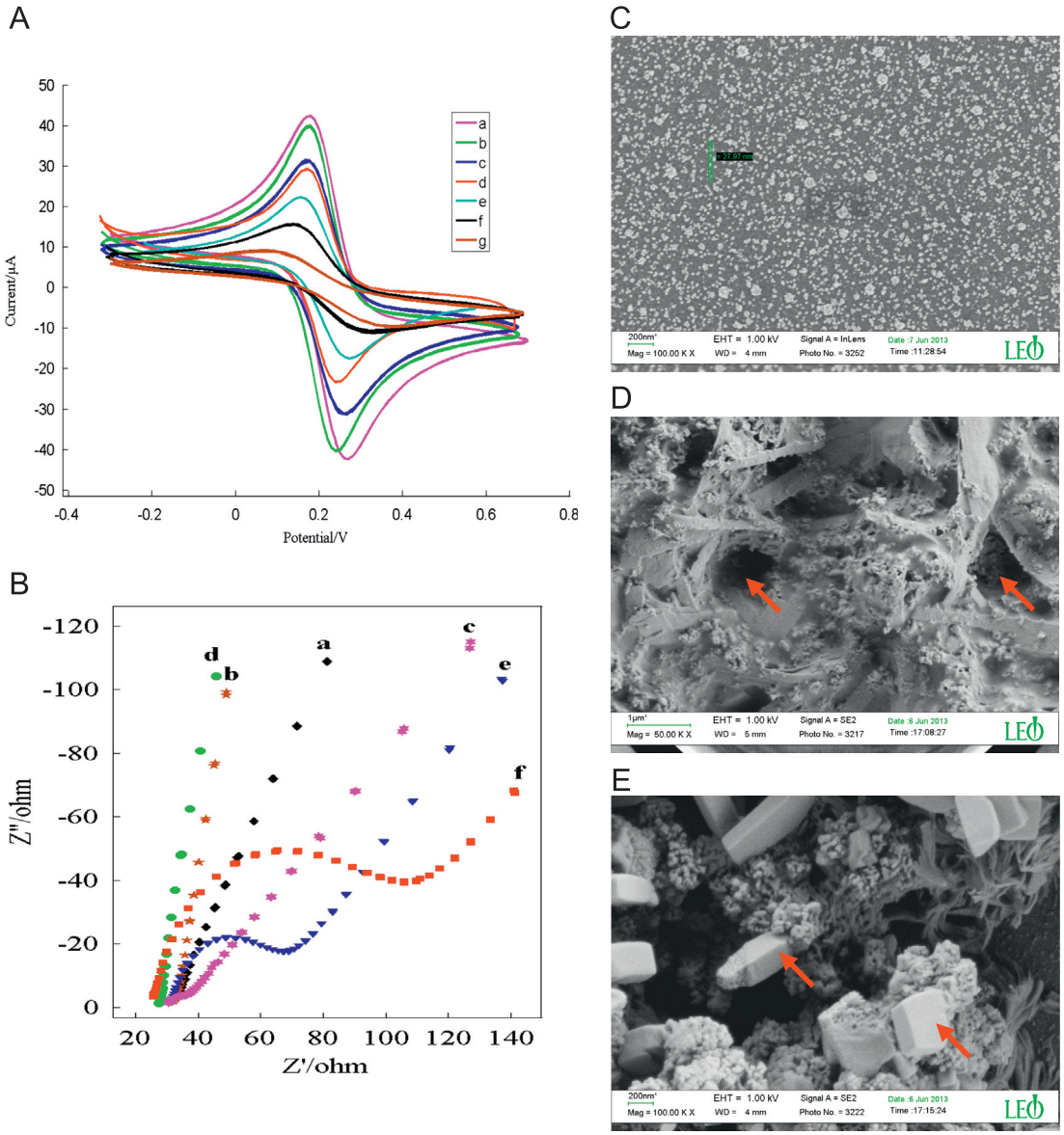

Fig. 1. CV scans; EIS and FESEM images of different electrodes made by modified fabrication processes. (A) (a) Second round of nano-Au electrodeposition; (b) blocking with 0.25% BSA; (c) first round of nano-Au electrodeposition; (d) nano-Au/ZnO sol–gel EPOR; (e) bare GCE; (f) nano-Au/ZnO sol–gel EPOR/nano-Au GCE detection EPO; and (g) rhEPO. (B) EIS for each modified step (a) bare GCE; (b) first round of nano-Au electrodeposition; (c) nano-Au/ZnO sol–gel EPOR; (d) second round of nano-Au electrodeposition; (e) blocking with 0.25% BSA; and (f) nano-Au/ZnO sol–gel EPOR/nano-Au GCE detection rhEPO. FESEM images of: (C) the first round of nano-Au electrodeposition, (D) ZnO sol–gel EPOR, and (E) the second round of nano-Au electrodeposition.

3. Results and discussion

3.1. Electrochemical characterization of the stepwise modified electrode

Fig. 1A shows the CV during the process of electrode modification. First, a standard CV was obtained with the unmodified GCE which was immersed in PBS standard solution (pH 7.4, 0.05 mol L^{-1}) containing 2 mmol L^{-1} $K_3[Fe(CN)_6]/K_4[Fe(CN)_6]$ (Fig. 1A, curve e); second, after the first round of nano-Au electrodeposition, the CV exhibits an obvious increase in peak current due to nano-Au promotion of electron transfer on the electrode surface (Han et al., 2012) (Fig. 1A, curve c); third, after fixation of ZnO sol–gel and EPOR on the nano-Au modified electrode surface, the CV exhibited an obvious decrease in the peak current, suggesting the fixation of ZnO sol–gel and EPOR onto the electrode surface and electron transfer deterring by the gel film on the electrode surface (Fig. 1A, curve d); fourth, after a second round of nano-Au electrodeposition, the CV showed a drastic increase in the peak current due to increased specific surface area and electron transfer of the electrode (Fig. 1A, curve a); fifth, after blockage of the modified electrode with BSA, the peak current decreased to a certain degree because of blockage of nonspecific absorptive sites and hindrance of electron transfer, when compared with the peak current after a second round of nano-Au electrodeposition (Fig. 1A, curve b); and lastly, the peak current of the modified, blocked working electrode further decreased after 20 min incubation in EPO (Fig. 1A, curve f) and rhEPO (Fig. 1A, curve g)-containing samples, because EPOR–EPO or EPOR–rhEPO complexes on the electrode surface impeded electron transfer substantially.

Due to the high affinity between ZnO sol–gel and nano-Au, ZnO sol–gel is fixed directly onto the nano-Au deposited electrode surface. ZnO sol–gel is characterized by a good chemical stability, thermal stability and biological compatibility, and it serves as a

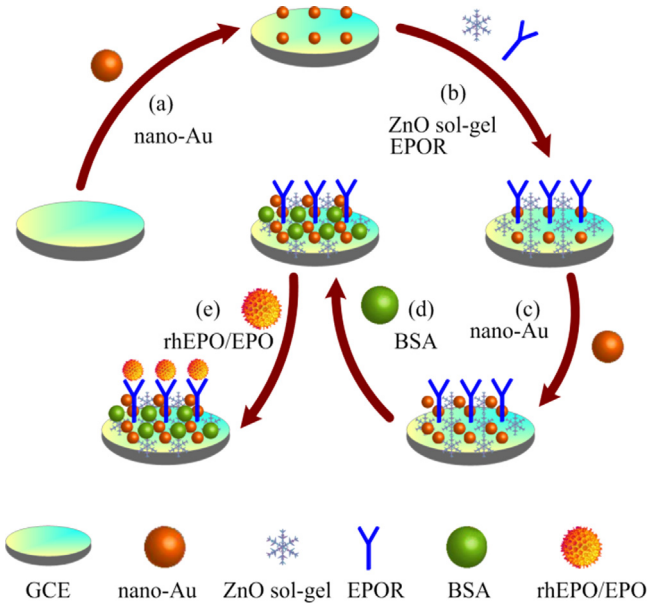

Scheme 1. Illustration of the stepwise electrochemical biosensor fabrication process. (a) First round of nano-Au electrodeposition; (b) assembled ZnO sol–gel EPOR; (c) second round of nano-Au electrodeposition; (d) blocking with 0.25% BSA; and (e) incubation with rhEPO/EPO.

good biocompatible interface for a second round of nano-Au deposition. Chemical absorption between nano-Au and sol–gel facilitated EPOR fixation. The nano-Au/ZnO sol–gel modified electrode prepared with this method provided a stable, compact surface for biological reactions, and doubled the load of EPOR fixed. Nevertheless, compared to unmodified nano-Au electrodes, the ΔI increased approximately 3-fold with the modified electrode after incubation with rhEPO/EPO containing samples (Fig. S1). The results suggest that this signal amplification method is simple and effective, and helps sensitive detection of trace rhEPO/EPO. This method not only increases detection sensitivity, but also reduces the detection time because there is no need for additional steps, e.g., PCR amplification (Ahmed et al., 2007; Xu et al., 2009; Xuan et al., 2012). Therefore, this method can be used for non-labeled, fast, real-time detection of rhEPO/EPO in sports games.

Electron-transfer resistance (Ret) at the electrode is an important parameter, thus electrochemical characteristics of the electrochemical biosensor was investigated by electrochemical impedance spectroscopy (EIS) measurements. It is well known that the semicircle diameter of EIS is equal to Ret in the Nyquist diagram. Fig. 1B illustrates the EIS of different electrodes. Bare GCE has a small semicircle in the high frequency section (curve a). For the electrode coated with nano-Au, the Nyquist diagram shows approximately a straight line (curve b), indicating nano-Au has excellent conductive properties. Then, following loading of ZnO sol–gel EPOR on the nano-Au /GCE, Ret increased compared to the bare GCE (curve c). The reason is that the ZnO sol–gel EPOR formed some barrier obstructing the electron transfer. Next, the Ret decreased obviously following a second round of nano-Au electrodeposition (curve d), due to the fact that the increased amount of nano-Au provides a large surface area and acts as a conducting tunnel to promote electron transfer. When blocked with 0.25% BSA, the semicircle increased markedly (curve e) because the capture BSA with its non-electroactive properties obstructs electron transfer. Ret further increases following successive rhEPO adsorption onto the electrode surface (curve f), which attributed to the inhibition effect of the BSA and EPOR–rhEPO biomacromolecules on electron transfer.

The surface images of the first round of nano-Au electrodeposition (Fig. 1C), nano-Au/ZnO sol–gel EPOR (Fig. 1D), and the second round of nano-Au electrodeposition (Fig. 1E) composite membrane was investigated by FESEM. As shown in Fig. 1C, after a first round of nano-Au electrodeposition, the nano-Au particles have a diameter ranging between 20 and 40 nm, and agglomeration can be found between partial nano-Au particles. Fig. 1D indicates a sparse porosity structure of the ZnO sol–gel (arrow). Fig. 1E shows the FESEM image after a second round of electrodeposition. As it shown, nano-Au crystals grow successfully on the surface of ZnO sol–gel film, with a diameter of approximately 200 nm (arrow).

3.2. Optimization of analytical conditions

The factors that influence the performance of the electrochemical biosensor have been discussed. As buffer's pH impacts EPOR–rhEPO/EPO activity significantly, we investigated the effect of pH on sensor performance. When solution's pH ranged between 3.8 and 9.0, the peak current of the modified electrode initially increases, and then decreases, with the highest peak current at pH 7.4 as shown in Fig. S2. Therefore, in the present study, phosphate buffer (pH 7.4) is chosen as our optimized buffer solution.

The incubation time is an important factor influencing biological reactions of the electrochemical sensor. At room temperature, the reduction peak current response of the nano-Au/ZnO sol–gel EPOR/nano-Au modified electrode decreases with extended receptor/ligand incubation and stabilizes after 20 min of incubation as shown in Fig. S3. Therefore, in the present study, the incubation time is set to 20 min.

3.3. Time optimization for nano-Au electrodeposition

3.3.1. The first round of nano-Au electrodeposition

Five sets of unmodified GCEs were immersed in 10 mmol L^{-1} $HAuCl_4$ solution for a 20 s, 40 s, 60 s, 80 s, and 100 s electrodeposition at a constant potential of 0.6 V. As shown in Fig. 2A, with increasing electrodeposition time, electrode's peak current increases drastically at first, and then decreases drastically. The peak current reaches its maximum at a deposition time of 60 s. The $HAuCl_4$ deposition time is an important factor that influences the layer thickness and the quantity of nano-Au deposited. Within a certain time range, the longer the electrodeposition time, the thicker the nano-Au layer deposited on the electrode surface, the higher is the peak current, and the higher the amplification efficiency. Nevertheless, if the electrodeposition time is too long, nano-Au layers that are too thick are deposited onto the electrode surface which will deter electron transfer. As shown in Fig. 2A, after 60 s of the first round of electrodeposition, sensor's current reaches its maximum. Therefore, 60 s of $HAuCl_4$ deposition time is decided to be the optimal nano-Au electrodeposition time.

3.3.2. The second round of nano-Au electrodeposition

Five sets of nano-Au/ZnO sol–gel EPOR-modified GCEs were immersed in 10 mmol L^{-1} $HAuCl_4$ solution for a second round of electrodeposition for 10 s, 20 s, 30 s, 40 s, and 50 s at constant potential of 0.6 V. As shown in Fig. 2B, as the electrodeposition time increases from 10 s to 30 s, electrode's peak current increases gradually; as the electrodeposition time increases from 30 s to 50 s, the peak current decreases gradually. These results indicate a maximum peak current at 30 s of electrodeposition time. After a second round of electrodeposition, a sandwich-like modification layer forms on the electrode surface. The thickness of the nano-Au layer formed after a second round of electrodeposition plays a crucial role in reactions of the receptors and analytes. The nano-Au layer is thin given a short electrodeposition time, which may affect the reactions of the receptors and analytes; in contrast, the nano-Au layer is thick given a long electrodeposition time, which may

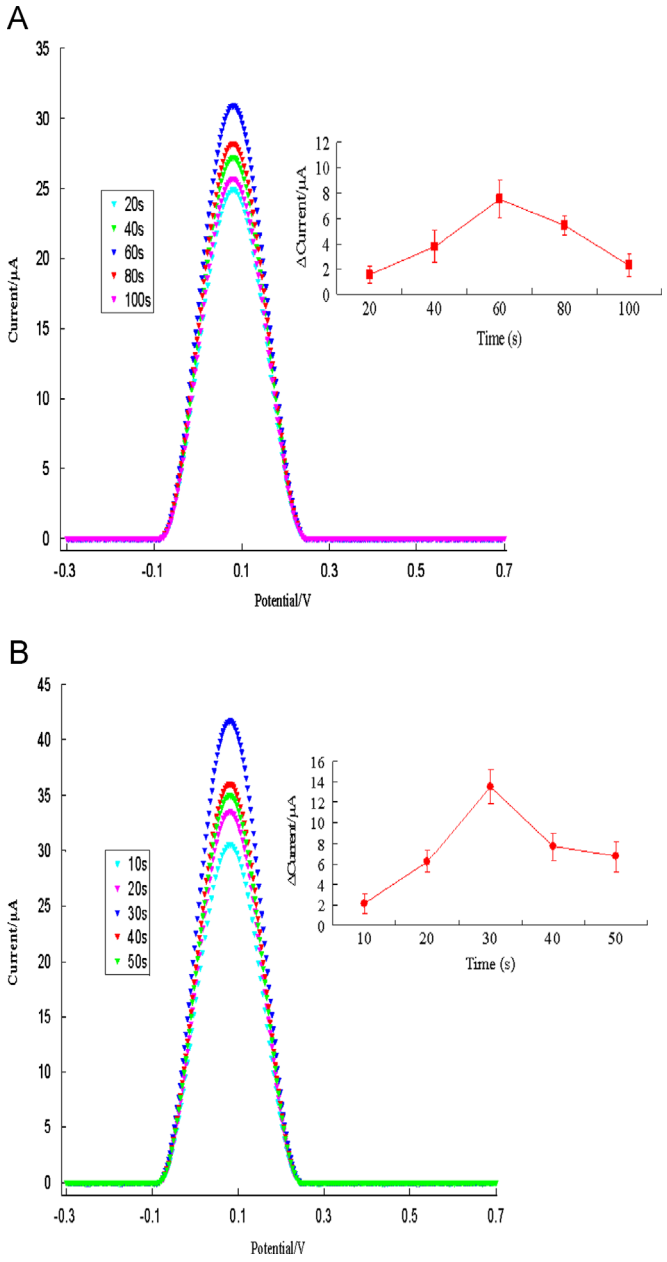

Fig. 2. CV scans of different periods of time on the (A) first and (B) second round of nano-Au electrodeposition on peak current of the GCE. Inset: plot of peak current signal in CV scans of different periods of time of the GCE. Mean values and standard deviations are obtained from at least three independent experiments.

affect electron transfer. As a trade-off, the optimal time for the second round of electrodeposition was set at 30 s.

3.4. Optimization of nano-Au concentration

Five sets of GCEs were immersed in 1, 5, 10, 15, and 20 mmol L^{-1} $HAuCl_4$ solution for electrodeposition at constant potential (first round of electrodeposition, 60 s; second round of electrodeposition, 30 s). As shown in Fig. 3, with the concentration of $HAuCl_4$ increasing, sensor's response current increases initially and then decreases, and the maximal response current is seen with 10 mmol L^{-1} $HAuCl_4$ solution. The response currents are low when electrodes were electrodeposited at other concentrations of the $HAuCl_4$ solution, possibly because the thickness and quantity of nano-Au deposited relates to the concentration of reduced chloroauric acid. Because nano-Au increases

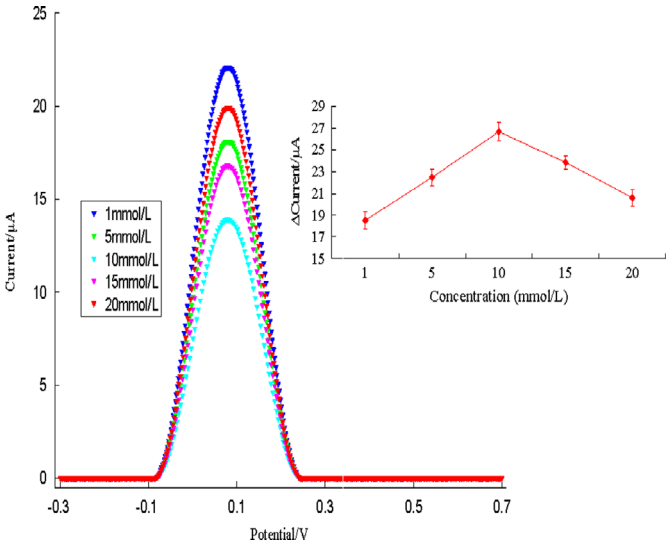

Fig. 3. CV scans of the reaction mixture containing different concentrations of $HAuCl_4$ solution after electrodeposition for 60 s and 30 s. Inset: plot of peak current signal in CV scans of different concentrations of $HAuCl_4$ solution. Mean values and standard deviations are obtained from at least three independent experiments.

electrode's specific surface area and the load of receptors, within a certain concentration range, a higher chloroauric acid concentration leads to a thicker nano-Au layer, thus helping electron transfer and amplification of biological reaction signals. Nevertheless, outside a certain concentration range, the thicker nano-Au layer hinders electron transfer, the higher nano-Au density on the electrode surface affects receptor fixation adversely. Therefore, 10 mmol L^{-1} chloroauric acid is decided to be the optimal concentration for electrodeposition.

3.5. Detection of rhEPO/EPO

The calibration plot for rhEPO/EPO detection with the Nano-Au-modified electrochemical biosensor is illustrated in Fig. 4. Under the optimal experimental conditions, various concentrations of rhEPO/EPO were detected. The results demonstrate that at the initial stage of the hybridization reaction, as EPOR–rhEPO/EPO complexes block the electron transfer channels on the electrode surface, the redox peak current decreases obviously when compared to the blank control. With the rhEPO/EPO concentration increasing, ΔI increases. As shown in Fig. 4A and B, when the rhEPO/EPO concentration ranges between 0.5 pg L^{-1} and 500 ng L^{-1}, there is a good linear relationship between the logarithmic concentration and peak current. For rhEPO, the linear regression equation is: $y=3.7068x+31.796$, and the correlation coefficient is 0.9912; for EPO, the linear regression equation is: $y=3.4389x+29.685$, and the correlation coefficient is 0.9925, for both rhEPO and EPO, the limit of detection is 0.1 pg L^{-1}. The results show that the electrochemical biosensor has a wider linear range and a lower limit of detection (Ho et al., 2009; Li H. et al., 2011; Tong et al., 2011; Li L. et al., 2012; Cao et al., 2013), when compared to the unmodified one.

3.6. Stability, reproducibility and anti-interference property

The stability of the electrochemical biosensor was also examined. As shown in Table S1, after storing for 10, 30, 50, 70, and 80 days ΔI was 97.45%, 94.33%, 83.29%, 75.07% and

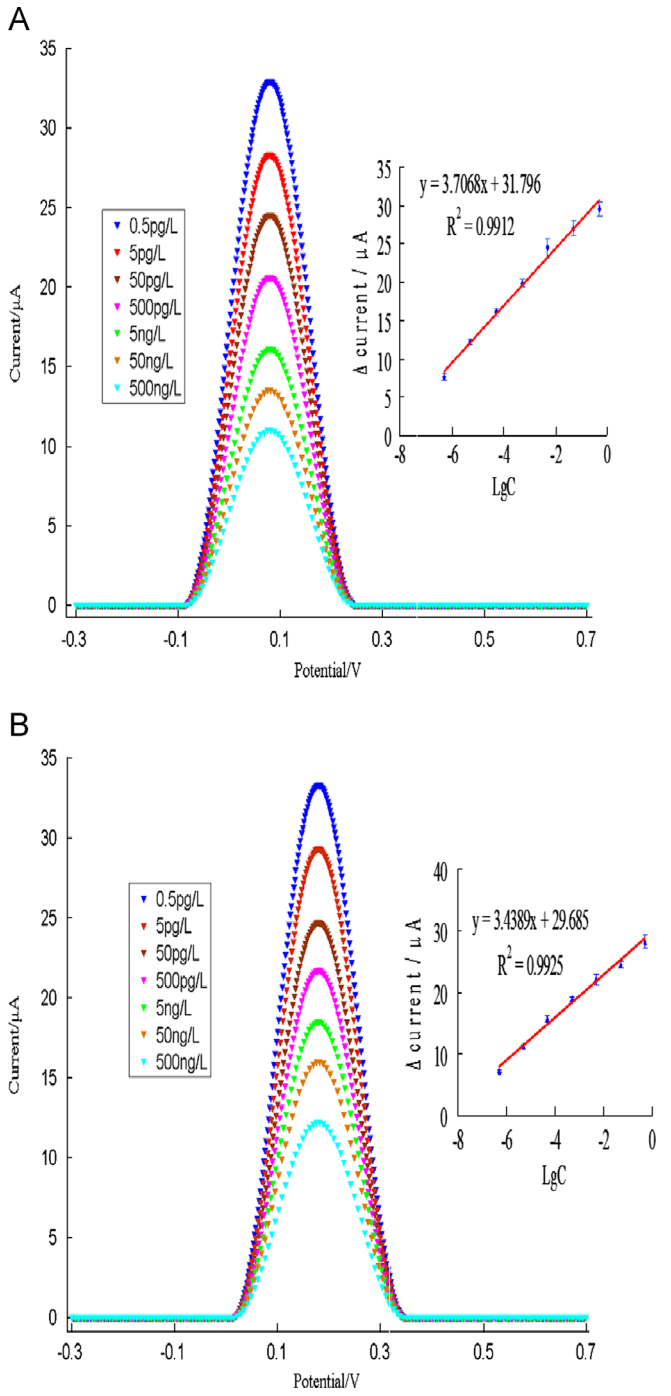

Fig. 4. Profiles of the electrochemical biosensor in the presence of different concentrations of (A) rhEPO and (B) EPO. From top to bottom: 0.5 pg L^{-1}, 5 pg L^{-1}, 50 pg L^{-1}, 500 pg L^{-1}, 5 ng L^{-1}, 50 ng L^{-1}, and 500 ng L^{-1} rhEPO/EPO. Inset: the calibration curve corresponding to the cyclic voltammetry quantitative detection of rhEPO or EPO with nano-Au/ZnO sol–gel/nano-Au modified electrochemical biosensor based on the changes of the ΔI. C: rhEPO or EPO concentration (μg L^{-1}), LgC: rhEPO or EPO denary logarithm. Mean values and standard deviations are obtained from at least three independent experiments.

25.21%, respectively, compared with the initial steady state value, suggesting a good long-term stability.

The reproducibility of the response of the electrochemical biosensor was evaluated by determining 0.1, 1.0 and 10.0 μg L^{-1} EPOR using six electrodes prepared in the same manner. For these three EPOR concentrations, the CV values were 2.22%, 2.25%, and 2.40% for intraday repeated assays, and were 4.32%, 4.17%, and 3.68% for interday repeated assays (Table S2). All CV values were less than 10%, suggesting a high reproducibility of our biosensors.

The specificity of the electrochemical biosensor plays a very important role in analyzing biological samples in situ. We studied five batches of modified electrodes with 500 ng L^{-1} rhEPO, EPO, rhEPO and interfering substances (500 ng L^{-1} IgA, IgG and IgM), EPO and 500 ng L^{-1} IgA, IgG and IgM, only 500 ng L^{-1} IgA, IgG and IgM, respectively. The current charge of ΔI is 29.50 μA, 28.63 μA, 27.31 μA, 26.42 μA and 0.53 μA respectively. These results show that the biosensor exhibited strong resistance to interference and was highly selective for rhEPO and EPO.

3.7. Clinical application

To further assess the clinical applicability of our biosensors, we determined serum rhEPO and EPO concentrations in a patient treated with rhEPO and a healthy volunteer. In brief, serum samples containing an electrolyte solution were subjected to CV scanning. According to the standard curves shown in Fig. 4A and B, the calculated rhEPO and EPO concentrations were 125 ng L^{-1} and 73 ng L^{-1}, respectively. Then, serum samples were diluted with ultrapure water, generating analyte solutions with various concentrations of rhEPO and EPO. Finally, the modified electrode was incubated 20 min in these analyte solutions, followed by CV scanning (see Table S3). As shown in Fig. S5, within the rhEPO concentration range of 0.125 ng L^{-1}–125 ng L^{-1}, and within the EPO concentration range of 0.073 ng L^{-1}–73 ng L^{-1}, the analyte concentration and the peak current exhibit a good linear relationship. For rhEPO, the equation of linear regression was: $y=3.647x+13.555$, with a correlation coefficient of 0.9893; for EPO, the equation of linear regression was: $y=3.180x+12.380$, with a correlation coefficient of 0.9891. The results demonstrate that our biosensors can be used in quantifying rhEPO and EPO in human serum samples.

3.8. Method comparison

In addition, the nano-Au/ZnO sol–gel/nano-Au signal amplification of the developed electrochemical biosensor for rhEPO/EPO detection has been compared with those of other signal amplification methods reported in the literatures. As shown in Table S4, our proposed electrochemical biosensor exhibits a relatively wider linear range, lower detection limit, and higher sensitivity, which provides evidence that our signal amplification is highly sensitive in the detection of rhEPO/EPO. In addition, the sandwich-type of nano-Au/ZnO sol–gel/nano-Au membrane greatly enhances the electrochemical signal, which improves the sensitivity of the electrochemical biosensor.

4. Conclusions

In the present study, we evaluated a novel, highly sensitive electrochemical biosensor for detection of trace rhEPO by fixing EPOR via nano-Au and ZnO sol–gel. This sensor is characterized by high sensitivity, a low limit of detection, and low cost. The main focus of the present study include extending the linear range and lowering the limit of detection of electrochemical biosensor detection, as well as amplification of sensor's detection signals, thus allowing detection of trace rhEPO. Compared to similar devices described in the literature, the nano-Au/ZnO sol–gel/nano-Au-modified electrode can be prepared easily and economically, and it exhibits a wide linear range and a low limit of detection (Li and Lin, 2007; Han et al., 2011; Li Y.J. et al., 2012; Wang et al.,

2012). The detection process with this biosensor is simple and fast, with an incubation time of only 22 min. Therefore, this biosensor is fully applicable to real-time detection of trace rhEPO in sports games in a fast, simple, sensitive, and specific manner.

Acknowledgments

This study was supported financially by the National Natural Science Foundation of China (81000776), Natural Science Foundation Project of CQ CSTC (2010BB5194), infectious diseases from Ministry of Health and Ministry of Science and Technology, China to XC (2008ZX10003-012), and a fund for the transformation of Scientific and Technological Achievements (2012XZH02) and Innovation Foundation of young talents (2010XQN26) of the Third Military Medical University.

Appendix A. Supporting information

Supplementary data associated with this article can be found in the online version at http://dx.doi.org/10.1016/j.bios.2013.06.038.

References

Ahmed, M.U., Idegami, K., Chikae, M., Kerman, K., Chaumpluk, P., Yamamura, S., Tamiya, E., 2007. Analyst 132, 431–438.
Arya, S.K., Saha, S., Ramirez-Vick, J.E., Gupta, V., Bhansali, S., Singh, S.P., 2012. Analytica Chimica Acta 737, 1–21.
Cao, X., Wang, N., Jia, S., Guo, L., Li, K., 2013. Biosensors and Bioelectronics 39, 226–230.
Cash, K.J., Ricci, F., Plaxco, K.W., 2009. Journal of the American Chemical Society 131, 6955–6957.
Deng, K., Xiang, Y., Zhang, L., Chen, Q., Fu, W., 2013. Analytica Chimica Acta 759, 61–65.
Gu, B., Xu, C., Yang, C., Liu, S., Wang, M., 2011. Biosensors and Bioelectronics 26, 2720–2723.
Han, J., Zhuo, Y., Chai, Y.Q., Mao, L., Yuan, Y.L., Yuan, R., 2011. Talanta 85, 130–135.
Han, J., Zhuo, Y., Chai, Y.Q., Yuan, Y.L., Yuan, R., 2012. Biosensors and Bioelectronics 31, 399–405.
Ho, J.A., Lin, Y.C., Wang, L.S., Hwang, K.C., Chou, P.T., 2009. Analytical Chemistry 81, 1340–1346.
Jeong, Y.C., Jung, B., Park, J.H., Park, J.K., 2012. Chemical Communications 48, 6378–6380.
Lasne, F., Martin, L., Crepin, N., de Ceaurriz, J., 2002. Analytical Biochemistry 311, 119–126.
Lasne, F., Martin, L., Martin, J.A., de Ceaurriz, J., 2007. International Journal of Biological Macromolecules 41, 354–357.
Lee, S.H., Sung, J.H., Park, T.H., 2012. Annals of Biomedical Engineering 40, 1384–1397.
Lei, Y., Yan, X., Zhao, J., Liu, X., Song, Y., Luo, N., Zhang, Y., 2011. Colloids and Surface B: Biointerfaces 82, 168–172.
Li, F., Feng, Y., Dong, P., Yang, L., Tang, B., 2011. Biosensors and Bioelectronics 26, 1947–1952.
Li, H., Wei, Q., He, J., Li, T., Zhao, Y., Cai, Y., Du, B, Qian, Z., Yang, M., 2011. Biosensors and Bioelectronics 26, 3590–3595.
Li, J., Lin, X.Q., 2007. Analytica Chimica Acta 596, 222–230.
Li, L., Wang, S., Yang, T., Huang, S., Wang, J., 2012. Biosensors and Bioelectronics 33, 279–283.
Li, X.M., Fu, P.Y., Liu, J.M., Zhang, S.S., 2010. Analytica Chimica Acta 673, 133–138.
Li, Y.J., Ma, M.J., Zhu, J.J., 2012. Analytical Chemistry 84, 10492–10499.
Liu, A.L., Zhong, G.X., Chen, J.Y., Weng, S.H., Huang, H.N., Chen, W., Lin, L.Q., Lei, Y., Fu, F.H., Sun, Z.L., Lin, X.H., Lin, J.H., Yang, S.Y., 2013. Analytica Chimica Acta 767, 50–58.
Liu, Z., Zhang, W., Zhu, S., Zhang, L., Hu, L., Parveen, S., Xu, G., 2011. Biosensors and Bioelectronics 29, 215–218.
Lubin, A.A., Plaxco, K.W., 2010. Accounts of Chemical Research 43, 496–505.
Mallorqui, J., Segura, J., de Bolos, C., Gutierrez-Gallego, R., Pascual, J.A., 2008. Haematologica 93, 313–314.
Palanisamy, S., Cheemalapati, S., Chen, S.M., 2012. Analytical Biochemistry 429, 108–115.
Takulapalli, B.R., 2010. ACS Nano 4, 999–1011.
Tan, Y., Deng, W., Chen, C., Xie, Q., Lei, L., Li, Y., Fang, Z., Ma, M., Chen, J., Yao, S., 2010. Biosensors and Bioelectronics 25, 2644–2650.
Tong, P., Zhang, L., Xu, J.J., Chen, H.Y., 2011. Biosensors and Bioelectronics 29, 97–101.
Tothill, I.E., 2009. Seminars in Cell and Developmental Biology 20, 55–62.
Wang, Y., Chen, M., Zhang, L., Ding, Y., Luo, Y., Xu, Q., Shi, J., Cao, L., Fu, W., 2009. Biosensors and Bioelectronics 24, 3455–3460.
Wang, C., Tan, X., Chen, S., Yuan, R., Hu, F., Yuan, D., Xiang, Y., 2012. Talanta 94, 263–270.
Wei, F., Liao, W., Xu, Z., Yang, Y., Wong, D.T., Ho, C.M., 2009. Small 5, 1784–1790.
Wei, Y., Li, Y., Liu, X., Xian, Y., Shi, G., Jin, L., 2010. Biosensors and Bioelectronics 26, 275–278.
Xu, W., Xue, X., Li, T., Zeng, H., Liu, X., 2009. Angewandte Chemie International Edition 48, 6849–6852.
Xuan, F., Luo, X., Hsing, I.M., 2012. Biosensors and Bioelectronics 35, 230–234.
Yeom, S.H., Kang, B.H., Kim, K.J., Kang, S.W., 2011. Frontiers in Bioscience 16, 997–1023.
Zhang, S., Hu, R., Hu, P., Wu, Z.S., Shen, G.L., Yu, R.Q., 2010. Nucleic Acids Research 38, e185.
Zhao, M., Huang, J., Zhou, Y., Chen, Q., Pan, X., He, H., Ye, Z., 2013. Biosensors and Bioelectronics 43, 226–230.